IOP Publishing Nanotechnology
Nanotechnology 26 (2015) 455203 (6pp) doi:10.1088/0957-4484/26/45/455203

Non-degenerate n-type doping by hydrazine treatment in metal work function engineered WSe_2 field-effect transistor

Inyeal Lee[1], Servin Rathi[1], Lijun Li[1], Dongsuk Lim[2], Muhammad Atif Khan[1], E S Kannan[3] and Gil-Ho Kim[1]

[1] Samsung-SKKU Graphene Center, Sungkyunkwan Advanced Institute of Nanotechnology (SAINT) and School of Electronics and Electrical Engineering, Sungkyunkwan University, Suwon 16419, Korea
[2] School of Advanced Materials Science and Engineering, Sungkyunkwan University, Suwon 16419, Korea
[3] Department of Physics, BITS-PILANI, K. K. BIRLA Goa Campus, Zuarinagar, Goa 403726, India

E-mail: ghkim@skku.edu

Received 11 August 2015, revised 10 September 2015
Accepted for publication 23 September 2015
Published 21 October 2015

Abstract

We report a facile and highly effective n-doping method using hydrazine solution to realize enhanced electron conduction in a WSe_2 field-effect transistor (FET) with three different metal contacts of varying work functions—namely, Ti, Co, and Pt. Before hydrazine treatment, the Ti- and Co-contacted WSe_2 FETs show weak ambipolar behaviour with electron dominant transport, whereas in the Pt-contacted WSe_2 FETs, the p-type unipolar behaviour was observed with the transport dominated by holes. In the hydrazine treatment, a p-type WSe_2 FET (Pt contacted) was converted to n-type with enhanced electron conduction, whereas highly n-doped properties were achieved for both Ti- and Co-contacted WSe_2 FETs with on-current increasing by three orders of magnitude for Ti. All n-doped WSe_2 FETs exhibited enhanced hysteresis in their transfer characteristics, which opens up the possibility of developing memories using transition metal dichalcogenides.

Keywords: WSe_2, n-doping, hydrazine treatment, metal work function, hysteresis

1. Introduction

For the past decade, graphene, a two-dimensional (2D) material, has been widely studied to realize fast and atomically thin field-effect transistors (FET) with unique electrical and mechanical properties such as high mobility, mechanical strength, and transparency and flexibility [1–3]. Inspired by graphene, new 2D materials based on transition metal dichalcogenides (TMDC) have been investigated owing to their unique layer-dependent physical properties. By varying the thickness of TMDCs, it is possible to tune their band gap and optical response as well as improve their on/off ratio [4, 5]. Another tremendous advantage of TMDCs over graphene is the availability of both n- and p-type materials in native forms —e.g., n-type MoS_2 and p-type WSe_2—which are highly desirable for complementary electronics [6]. However, one of the crucial challenges in realizing high-performance TMDC-based FETs is to obtain good ohmic contact and control the doping state in these materials. In the past, several metals have been studied for contact engineering in TMDC-based FETs [7]. Further, various doping techniques for TMDCs were used such as metal ion decorated DNA treatment (p-doping) [8], silicon nitride passivation (n-doping) [9], and exposure to nitrogen dioxide (p-doping) [10] and potassium (n-doping) vapour [11]. However, a combined study of the doping effect and contact engineering, which would provide a better understanding of the device operation in TMDC-based electronics with various metals, is still missing.

In this work, we fabricated few-layer WSe_2 FETs with different contact metals (Ti, Co, and Pt) with significant differences in work function and investigated the chemical doping effect by hydrazine solution. Our n-doping process by the dipping method in solution is facile and simple compared to other methods [8–11]. The results show that for Ti- and Co-contacted FETs, hydrazine treatment makes them strongly n-type, and for Pt-contacted FETs, the pristine p-type was converted to n-type.

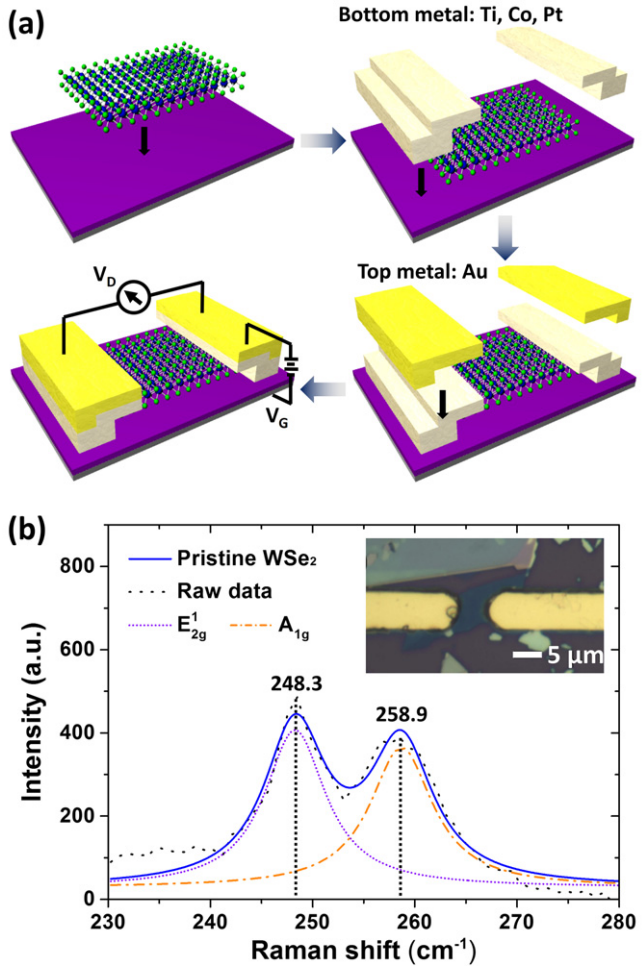

Figure 1. (a) Schematic of the WSe_2 FET fabrication process. (b) Raman spectrum of a thin WSe_2 layer used in this study. Inset shows the optical image of a fabricated WSe_2 FET.

2. Experimental details

Figure 1(a) shows schematics of the WSe_2 FET fabrication process. The WSe_2 thin layer was exfoliated from bulk and deposited on 90 nm thick SiO_2/Si substrate. The electrodes were patterned by optical lithography. A 20 nm thick layer of Ti, Co, or Pt was first deposited as a contacting metal layer on the patterned WSe_2 layer, followed by 50 nm thick Au for an electrode pad. The inset in figure 1(b) shows the optical image of a fabricated WSe_2 FET. The channel length and width of the fabricated devices were approximated by electrode gap size and metal electrode width—i.e., 5 μm and 5 μm, respectively. All electrical characterisations were performed by three-terminal measurement with the channel current controlled using the back gate. In the following discussions, each device with a specific contacting metal is designated as Ti–WSe_2, Co–WSe_2, or Pt–WSe_2. The WSe_2 layer on SiO_2/Si substrate was identified by Raman spectroscopy, as shown in figure 1(b). The peak positions of the in-plane mode (E^1_{2g} at 248.3 cm^{-1}) and out-of-plane mode (A_{1g} at 258.9 cm^{-1}) are in good agreement with the previous report on thin WSe_2 layers [12].

3. Results and discussion

3.1. Electrical properties of pristine WSe_2 FETs with different metal contacts

Figures 2(a) and (b) are plots of the transfer characteristics (I_D–V_G) of the Ti–, Co–, and Pt–WSe_2 FETs in linear and logarithm scales. It can be seen that the electrical characteristics vary significantly with the contacting metals, which have different work functions of 4.3, 5.0, and 5.7 eV for Ti, Co, and Pt, respectively [13]. The Pt–WSe_2 FET shows a unipolar p-type behaviour with a threshold voltage (V_{th}) at 6 V whereas Co–WSe_2 and Ti–WSe_2 FETs show ambipolar behaviour with V_{th} at −11 and −7 V, respectively. Although the Ti– and Co–WSe_2 FETs show quasi-ambipolar behaviour, the conductions were dominated by electrons rather than by holes. The on-currents of Pt– and Co–WSe_2 were approximately 10^{-5} A, which is three orders of magnitude higher than that of Ti–WSe_2, as shown in figure 2(c). (For further analysis of I_D–V_D characteristics, see supplementary information figure S1 and related discussion.) This variation in conduction carrier type and current magnitude can be explained by the difference in the contact (or Schottky) barrier height at the metal–WSe_2 interface [5]. Because TMDC-based 2D materials have unique surface properties, free from dangling bonds and surface states, this clean interface suits the Schottky theory rather than the Bardeen theory, which is based on Fermi level pinning because of surface states and dangling bonds as commonly observed in bulk semiconductors such as silicon- and germanium-based devices [14, 15]. In figure 2(d), band alignments of the conduction and valence bands (CB and VB) of WSe_2 with the work function of metals are indicated [16, 17]. In case of Ti contact, the work function lies near the CB; consequently, a high hole barrier (ϕ_{bp}) was formed. In contrast, the work functions of Co and Pt metals are closer to the VB, which results in a high electron barrier (ϕ_{bn}) and relatively low ϕ_{bp}. From the band diagram, Ti–WSe_2 is expected to have low electron/hole conduction whereas the conductions of Co– and Pt–WSe_2 are expected to be dominated by holes. In the case of Ti– and Pt–WSe_2, the measured electrical results are in agreement with the prediction; however, the Co–WSe_2 shows an unexpectedly high electron conduction. This high electron conduction was also observed in several Co–WSe_2 FETs fabricated separately, suggesting the possibility that the Fermi level of Co metal was pinned near the CB of WSe_2.

The field-effect mobility was extracted from the linear I_D–V_G curve at $V_D = 1$ V, using expression

$$\mu = \frac{L}{W}\left(\frac{dI_D}{dV_G}\right)\left(\frac{1}{C_i \times V_D}\right), \quad (1)$$

where W and L are the channel width and length, respectively, and $C_i = 38\ \mathrm{nF\,cm^{-2}}$ is the capacitance per unit area between the gate and the channel layer. The mobility values are 3.12×10^{-5}, 0.55, and 9.16 $cm^2\,V^{-1}\,s^{-1}$ for Ti–, Co–, and Pt–WSe_2 FETs, respectively. Because the fabrication conditions and exfoliated layers were similar for all samples, the variation observed in mobility can be attributed

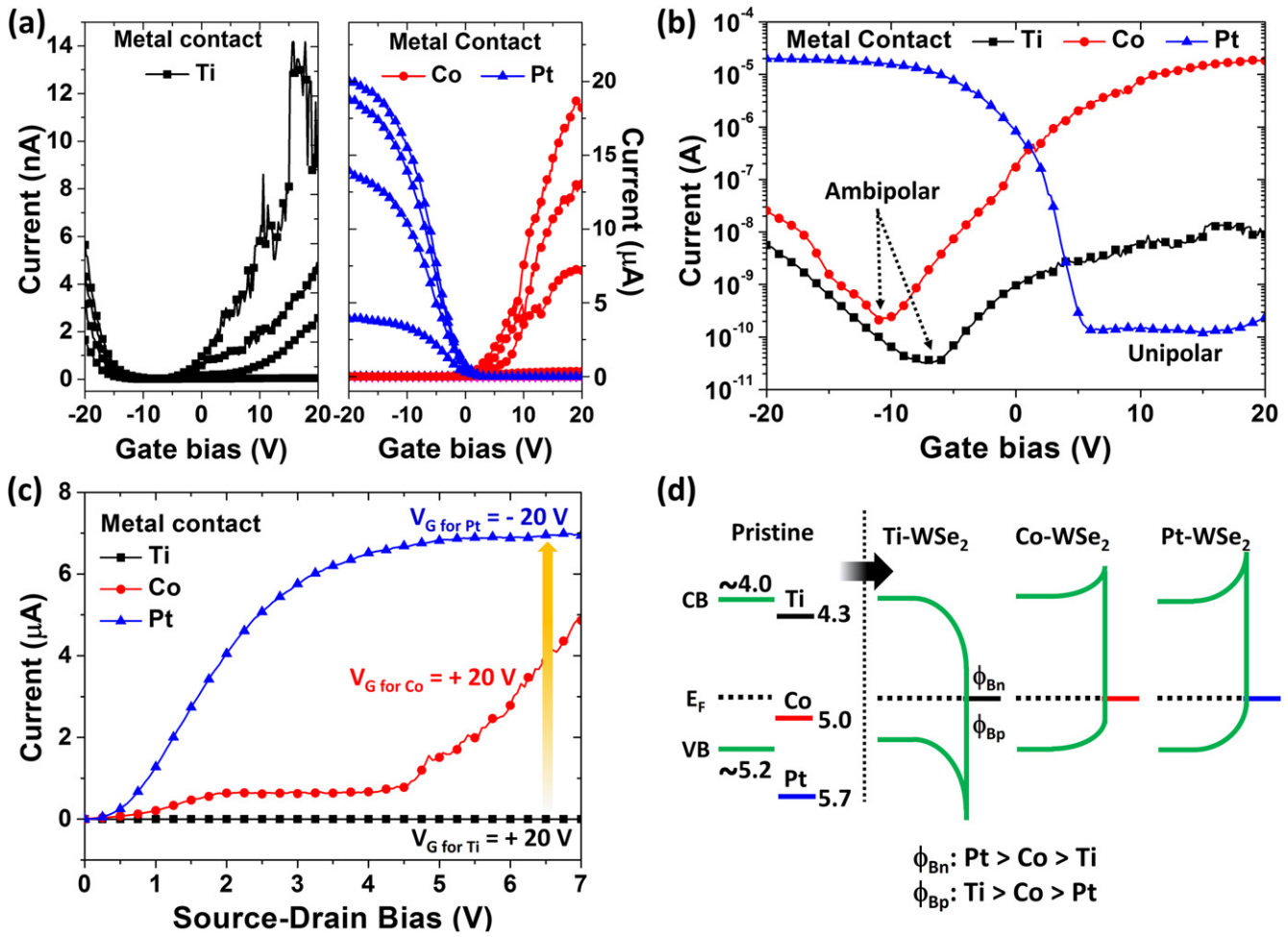

Figure 2. I_D–V_G characteristics for Ti–, Co–, and Pt–WSe_2 FETs in (a) linear scale with V_D from 1 to 7 V with 2 V steps and (b) logarithm scale with V_D = 7 V. (c) I_D–V_D characteristics with gate bias at on-current state. (d) Schematic of band diagram for Ti–, Co–, and Pt–WSe_2 FETs before and after band alignment, where ϕ_{bn} and ϕ_{bp} indicate electron and hole contact barriers, respectively. The unit of CB, VB, and E_F is eV.

to the effect of the contact resistance. Devices fabricated using Pt contact showed the highest mobility compared to the devices with Ti and Co contacts because Pt exhibited the lowest contact resistance. Consequently, the on/off ratio takes values of 10^3, 10^4, and 10^5 for Ti–, Co–, and Pt–WSe_2 FETs, respectively. From the measured transport properties, Pt and Co metals proved to be a suitable contact for improving the electrical performance of p- and n-type transport in WSe_2 FETs, respectively, whereas the Ti-contacted WSe_2 FET exhibited low electrical performance for both electron and hole transport.

3.2. Electrical properties of hydrazine-treated WSe_2 FETs with different metal contacts

Having identified the work function dependence of the contact metal, we investigate the surface doping effect of hydrazine monohydrate on the WSe_2 FET. The Ti–, Co–, and Pt–WSe_2 FETs were dipped in hydrazine solution with a concentration of 80% for 20 s to achieve the n-doped property of the WSe_2 layer, as shown in figure 3(a). Because hydrazine, also known as diazane, is composed of two amine molecules, it has a strong tendency to donate electrons to the WSe_2 surface, making the channel predominately n-type as shown in figure 3(b). A similar charge transfer mechanism has also been demonstrated in graphene and carbon nanotube-based devices [18, 19]. This doping mechanism can also be verified from the redox potential values. As illustrated in figure 3(c), the CB edge energy of WSe_2 at neutral pH lies at approximately −0.25 eV versus the standard hydrogen electrode, which is much smaller than the standard reduction potential of hydrazine (−1.16 V) [20, 21]. As a result, the electrons from hydrazine are donated to WSe_2, thereby achieving n-doping in WSe_2 FETs. This doping was further confirmed by the Raman analysis. Figure 3(d) shows the Raman spectra for untreated and treated WSe_2 layers in the hydrazine solution. After hydrazine treatment, the E^1_{2g} and A_{1g} modes slightly shifted to a lower frequency with peak positions at 248.0 and 258.5 cm^{-1}. This is in good agreement with the previously reported n-doped WSe_2 layer [9], although the shifts are less significant because the material in this study is not mono- or bilayer. In thick TMDC layers, the layers closer

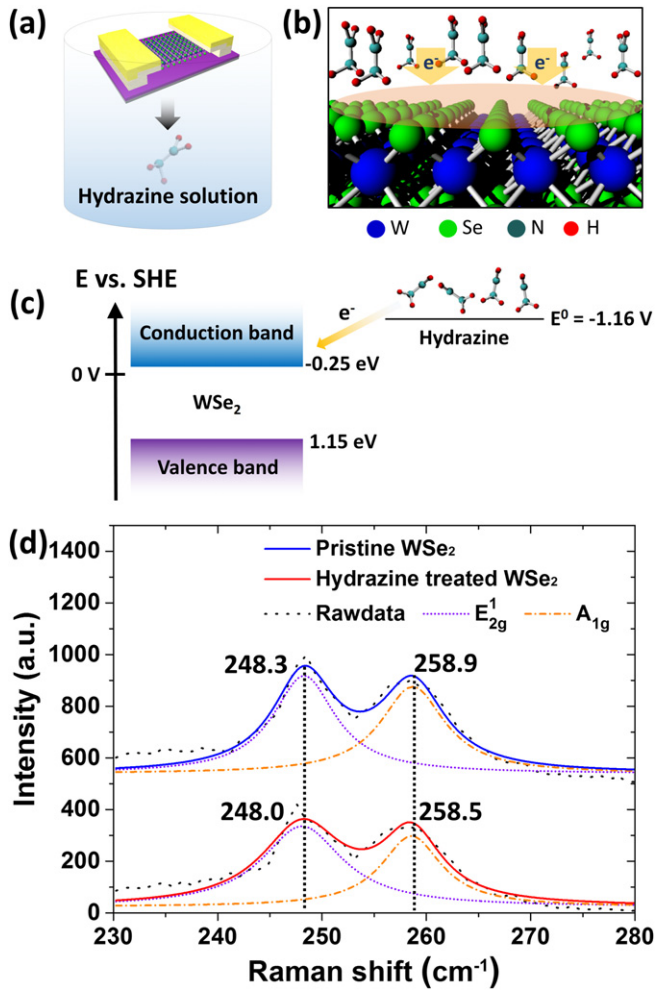

Figure 3. Schematics of (a) hydrazine treatment method and (b) the mechanism of the hydrazine-based doping process. (c) Doping mechanism in multi-layered WSe_2. (d) Raman spectra of the WSe_2 layer before and after hydrazine treatment.

to the surface are more effectively doped compared to the layers far from the surface, which explains the smaller Raman shift observed in our measurement [22].

The I_D–V_G characteristics of hydrazine-treated WSe_2 FETs are shown in figures 4(a)–(c). In the case of the Ti–WSe_2 FET (figure 4(a)), the threshold voltage shifted from −7 to beyond −20 V, indicating a heavily n-doped channel with current and mobility increasing by three orders of magnitude compared to the untreated Ti–WSe_2 FET—i.e., from 3.12×10^{-5} to $0.01\ cm^2\ V^{-1}\ s^{-1}$. Similarly, the Co–$WSe_2$ FET also shows a shift of V_{th} from −11 to approximately −20 V with roughly same on-current of 10^{-5} A, as shown in figure 4(b). However, the mobility of the hydrazine-treated Co–WSe_2 FET slightly decreases from 0.55 to $0.38\ cm^2\ V^{-1}\ s^{-1}$. Interestingly, in the case of the Pt–WSe_2 FET (figure 4(c)), the initial p-type WSe_2 FET was converted to n-type after treatment, with a decrease of on-current from 10^{-5} to 10^{-7} A and effective mobility from 9.16 to $0.07\ cm^2\ V^{-1}\ s^{-1}$. It may be noted that the value of the effective mobility is the combination of the intrinsic mobility and the quality of the ohmic contact; i.e., if the contact resistance is higher than for the similar intrinsic mobility, the observed field-effect mobility would decrease. Therefore, the increase in the field-effect mobility in the Ti–WSe_2 FET could have its origin from the improvement in the contact resistance after hydrazine treatment.

The observed electrical properties can be explained by the shift of the Fermi level from the vicinity of VB to CB, as shown in figure 4(d). The quasi position of the Fermi level can be calculated by using typical semiconductor carrier density equations [23]. However, in the case of two-terminal measurement, where contact resistance cannot be excluded from the channel resistance, such analysis can lead to erroneous conclusions. In view of this limitation, a qualitative analysis has been employed to study the observed variation in the device characteristics. (For a detail discussion on this issue, see supplementary information, section 2). The up-shift in the Fermi level of WSe_2 due to n-doping treatment lowers the barrier for electron injection, which results in higher on-current and enhanced mobility in the Ti–WSe_2 FET. In the case of Co– and Pt–WSe_2 FETs, a relatively higher ϕ_{bn} was formed, which results in lower on-current and mobility compared to the Ti–WSe_2 FET. In contrast, ϕ_{bp} was highly increased; consequently, the hole transport vanished after the n-doping process. Furthermore, n-type doping in the Ti–WSe_2 FET shows weak degenerate behaviour whereas for Co and Pt contacts, it was possible to modulate the total carrier concentration by gate bias owing to higher barrier height for electron conduction. Finally, the doped devices also showed enhanced hysteresis behaviour, which can be utilized for memory applications. (For details, see supplementary information figure S3 and the related discussion.) From the analyzed electrical measurements, we found that high performance of the n-type WSe_2 FET can be achieved with (1) a low work function (near the CB of WSe_2) metal contact (Ti in this study), and (2) n-doping by using a hydrazine treatment. The results reveal not only the importance of contact engineering to improve device performance but also the critical role of facile doping in 2D materials, which can extend the device functionality for various applications such as digital and optoelectronics.

4. Conclusion

In conclusion, we studied WSe_2 FETs with various metal contacts using Ti, Co, and Pt and applied a facile hydrazine treatment method to realize high performance of n-type WSe_2 FETs. We analyzed the contribution from the metal work function to the electrical properties before and after n-doping treatment. After the n-doping treatment, the Ti– and Co–WSe_2 FETs showed a highly n-doped behaviour with enhanced electron conduction and negatively shifted V_{th}, whereas the p-type Pt–WSe_2 was changed to an n-type FET. This doping treatment can be utilized to realize complimentary devices and logic circuits based on atomically thin TMDC materials.

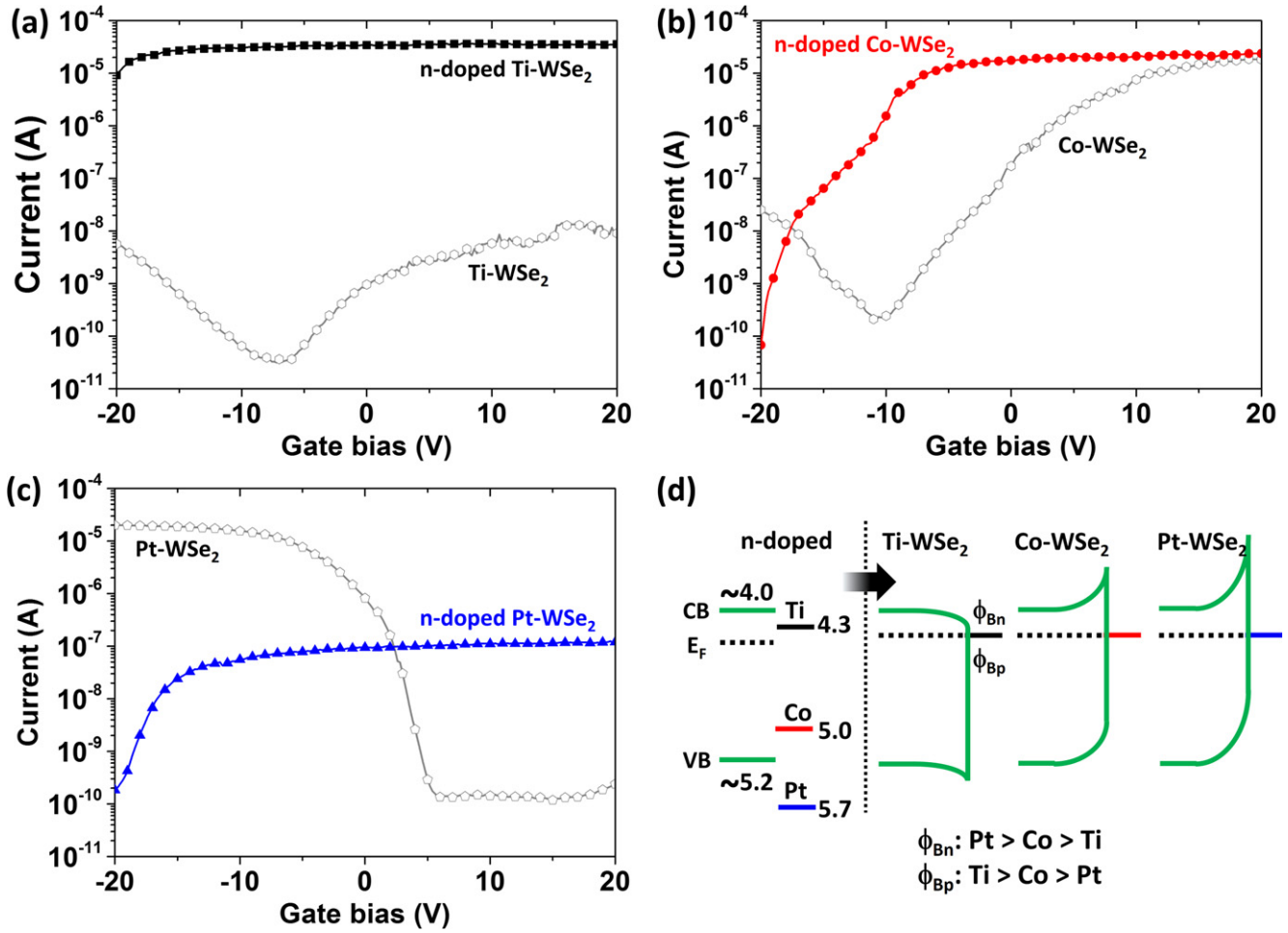

Figure 4. I_D–V_G characteristics before and after hydrazine treatment of (a) Ti–, (b) Co–, and (c) Pt–WSe_2 FETs with V_D at 7 V. (d) Schematic of the band diagram for hydrazine-treated Ti–, Co–, and Pt–WSe_2 FETs before and after band alignment, where ϕ_{bn} and ϕ_{bp} indicate electron and hole contact barriers, respectively. The unit of CB, VB, and E_F is eV.

Acknowledgments

This research was supported by Basic Science Research Program through the National Research Foundation of Korea (NRF) funded by the Ministry of Education, Science and Technology (2013R1A2A2A01069023).

References

[1] Geim A K and Novoselov K S 2007 The rise of graphene *Nat. Mater.* **6** 183–91
[2] Park J, Kang H, Chung D, Kim J, Kim J G, Yun Y, Lee Y H and Suh D 2015 Dual-gated BN-sandwiched multilayer graphene field-effect transistor fabricated by stamping transfer method and self-aligned contact *Curr. Appl. Phys.* **15** 1184–7
[3] Lee Y and Ahn J 2013 Graphene-based transparent conductive films *Nano* **8** 1330001
[4] Radisavljevic B, Radenovic A, Brivio J, Giacometti V and Kis A 2011 Single-layer MoS_2 transistors *Nat. Nanotechnology* **6** 147–50
[5] Huang J K, Pu J, Hsu C L, Chiu M H, Juang Z Y, Chang Y H, Chang W H, Iwasa Y, Takenobu T and Li L J 2014 Large-area synthesis of highly crystalline WSe_2 monolayers and device applications *ACS Nano* **8** 923–30
[6] Cho A J, Park K C and Kwon J Y 2015 A high-performance complementary inverter based on transition metal dichalcogenide field-effect transistors *Nanoscale Res. Lett.* **10** 115
[7] Liu W, Kang J, Sarkar D, Khatami Y, Jena D and Banerjee K 2013 Role of metal contacts in designing high-performance monolayer n-type WSe_2 field effect transistors *Nano Lett.* **13** 1983–90
[8] Park H Y, Dugasani S R, Kang D H, Jeon J, Jang S K, Lee S, Roh Y, Park S H and Park J H 2014 n- and p-type doping phenomenon by artificial DNA and M-DNA on two-dimensional transition metal dichalcogenides *ACS Nano* **8** 11603–13
[9] Chen K, Kiriya D, Hettick M, Tosun M, Ha T J, Madhvapathy S R, Desai S, Sachid A and Javey A 2014 Air stable n-doping of WSe_2 by silicon nitride thin films with tunable fixed charge density *APL Mater.* **2** 92504
[10] Fang H, Chuang S, Chang T C, Takei K, Takahashi T and Javey A 2012 High-performance single layered WSe_2 p-FETs with chemically doped contacts *Nano Lett.* **12** 3788–92
[11] Fang H, Tosun M, Seol G, Chang T C, Takei K, Guo J and Javey A 2013 Degenerate n-doping of few-layer transition metal dichalcogenides by potassium *Nano Lett.* **13** 1991–5

[12] Zao W, Ghorannevis Z, Amara K K, Pang J R, Toh M, Zhang X, Kloc C, Tan P H and Eda G 2013 Lattice dynamics in mono- and few-layer sheets of WS_2 and WSe_2 *Nanoscale* **5** 9677–83

[13] Stanislaw H and Tomasz D 1998 Work functions of elements expressed in terms of the Fermi energy and the density of free electrons *J. Phys.: Condens. Matter* **10** 10815–26

[14] Toshishige Y 2006 Equivalent circuit model for carbon nanotube Schottky barrier: influence of neutral polarized gas molecules *Appl. Phys. Lett.* **88** 083106

[15] Toshishige Y 2004 Modeling of carbon nanotube Schottky barrier modulation under oxidizing conditions *Phys. Rev.* B **69** 125408

[16] Kyounghwan K, Stefano L, Babak F, Kayoung L, Jiamin X, David C D, Chris M C and Emanuel T 2015 Band alignment in WSe_2–graphene heterostructures *ACS Nano* **9** 4527–32

[17] Hailong Z *et al* 2015 Large area growth and electrical properties of p-type WSe_2 atomic layers *Nano Lett.* **15** 709–13

[18] Lee I Y, Park H Y, Park J, Lee J, Jung W S, Yu H Y, Kim S W, Kim G H and Park J H 2013 Hydrazine-based n-type doping process to modulate Dirac point of graphene and its application to complementary inverter *Org. Electron.* **14** 1586–90

[19] Maiti U N, Lee W J, Lee J M, Oh Y, Kim J Y, Kim J E, Shim J, Han T H and Kim S O 2014 25th anniversary article chemically modified/doped carbon nanotubes and graphene for optimized nanostructures & nanodevices *Adv. Mater.* **26** 40–67

[20] Wang W N, Soulis J, Yang Y J and Biswas P 2014 Comparison of CO_2 photoreduction systems: a review *Aerosol Air Qual. Res.* **14** 533–49

[21] Park J W, Chae E H, Kim S H, Lee J H, Kim J W, Yoon S M and Choi J Y 2006 Preparation of fine Ni powders from nickel hydrazine complex *Mater. Chem. Phys.* **97** 371–8

[22] Dhakal K P, Duong D L, Lee J, Nam H, Kim M, Kan M, Lee Y H and Kim J 2014 Confocal absorption spectral imaging of MoS_2: optical transitions depending on the atomic thickness of intrinsic and chemically doped MoS_2 *Nanoscale* **6** 13028–35

[23] Sze S M 1981 *Physics of Semiconductor Devices* (New York: Wiley)